AERODYNAMIC MODELLING IN RE-ENTRY ANALYSIS BASED ON ON-GROUND FREE-FLIGHT TESTING WITHIN THE TEMIS-DEBRIS PROJECT

Patrick M. Seltner, Thorn Schleutker, Pawel Goldyn, Niklas Wendel, Ali Guelhan

German Aerospace Center (DLR)
Supersonic and Hypersonic Technologies Department of the Institute of Aerodynamics and Flow Technology
Linder Hoehe, 51147 Cologne, Germany

ABSTRACT

An empirical fragment-flow interaction model for the atmospheric entry of space debris is developed in this study. This aerodynamic model represents both the influence of the unsteady flight attitude and the aerodynamic interactions between multiple bodies on the motion of debris fragments. At DLR's H2K in Cologne, series of free-flight tests were performed using various common geometries such as spheres, spherical caps, boxes, plates, cylinders, cones and more complex bodies as test articles. Stereo tracking was applied to measure high-speed 6DoF motion data. Motion derivatives and aerodynamic coefficients were determined in a comprehensive data processing. Trigonometric series were fitted on the coefficient data as a function of pitch angle and aspect ratio. The results of cylinders are shown in this paper.

Index Terms— Re-entry trajectory, High-speed aerodynamics, Aerodynamic interactions, Hypersonic wind tunnel, Free-flight technique

1. INTRODUCTION

As the number of objects in Earth orbits is increasing disproportionately with a growing number of commercial launches and new satellite constellations [1], the mitigation and avoidance of space debris is becoming increasingly relevant. Remaining space objects, especially in low Earth orbit, pose a critical threat to upcoming space flights and active satellites due to the risk of collision. For this reason, ESA's new Space Debris Mitigation Guidelines aim to reduce the residence time after end-of-life and to lower on-ground casualty risk caused by space debris [2]. Re-entry analysis tools and their aerodynamic modelling are also becoming more important to make the prediction of impact footprints and thus the casualty risk assessment more accurate in order to protect people and property from harm. In doing so, the experimental database and modelling capabilities for the aerodynamic behaviour of debris fragments during re-entry into the atmosphere are limited, especially with regard to the influence of body orientation and the interaction of multiple bodies.

According to the study by Passey and Melosh [3], several different effects contribute to the scattering of multiple fragments after atmospheric breakup, with the gravity, the lift force of the single fragment and the aerodynamic interaction of several bow shocks being the dominant causes. Aerodynamic lift forces arise for the single fragment due to their non-spherical body shape, which can lead to a lateral separation depending on the direction of lift. In the research activities of the past decade (e.g. [4, 5, 6, 7, 8, 9, 10, 11]), the aerodynamic interactions of multiple objects have gained importance with respect to the fragmentation, demise and separation behaviour of space debris objects entering the atmosphere, as these phenomena influence their flight trajectories, velocities and masses.

As part of the interdisciplinary project "Technologies for Mitigation of Space Debris" (TEMIS-DEBRIS) of the German Aerospace Center (DLR), experimental studies have been performed to analyse the aerodynamic behaviour of single and multiple fragments of space debris during atmospheric entry. Aerodynamic interactions such as shock-shock interaction and wake-shock interaction are also highly relevant in this context [12], as they affect the flight trajectories with high separation velocities in the case of shock-wave surfing [13]. The knowledge gained can be used to predict the trajectories of debris fragments as they enter the atmosphere and to assess their impact footprint with regard to re-entry analysis tools.

Several solid objects, including spheres, spherical caps, boxes, plates, cylinders, cones and more complexes bodies, have been studied in the Hypersonic Wind Tunnel Cologne (H2K) at the DLR. In doing so, test articles with different aspect ratios are also part of this work. Free-flight tests with single bodies, covering the full range of pitch angles, have been conducted, while balance measurements with a free-falling and a fixed-mounted body in various relative positions and orientations are planned. The free-flight technique enables a continuous rotation of the bodies without any sting interferences in a broad angular range. In order to determine the aerodynamic loads, a high-speed stereo-tacking measurement technique has been used for the single-body tests and a force

moment-type balance instrumentation will be applied for the multi-body tests. The stereo tracking also provides 6-degrees-of-freedom (6DoF) data of the models' positions and orientations to analyse their motion behaviour. In addition, schlieren videography has been employed to visualize the flow topology.

On the basis of experimental data, complete aerodynamic databases or rather mathematical functions for the aerodynamic coefficients as a function of pitch angle and relative position (for multi-body arrangements) are to be determined for different body shapes by means of regression analyses. These aerodynamic databases will be used in an aerodynamic model as a two-body problem, assuming no impact of the trailing fragment on the leading one. The single-body data applies to leading fragments and intact objects of space debris before breakups, while the multi-body data is used for trailing fragments. The advantage of this new model is that both the influence of orientation and the interaction between multiple bodies on the motion of the debris fragments are considered. Furthermore, the superposition of aerodynamic coefficients for complex geometries based on the coefficients of simple solid objects will be investigated and considered for this aerodynamic model. The resulting aerodynamic model based on the experimental data will then be used for flight dynamic simulations of a satellite reference configuration using Modia3D [14, 15] modified by methods of the DLR Environment Library [16]. This is part of another work package of the TEMIS-DEBRIS project.

2. EXPERIMENTAL MODELS & METHODS

The experimental setup and data processing for the single-body tests were essentially the same as in previous work, which is described in [17, 18].

2.1. Hypersonic Wind Tunnel Cologne (H2K)

All experiments were performed in the Hypersonic Wind Tunnel Cologne H2K, which is located at the Supersonic and Hypersonic Technologies Department of DLR. This test facility is an intermittently working blowdown facility that comprises pressure vessels, a settling chamber, axisymmetric contoured Laval nozzles for fixed design Mach numbers of 5.3, 6.0, 7.0, 8.0, 8.7 and 11.2, a cylindrical free-jet test section with several optical accesses, a water-cooled diffuser and a vacuum sphere. At the nozzle exit, the diameter is 600 mm, while the axially symmetrical homogeneous core flow has an average diameter of about 420 mm. In the core flow, the maximum deviation of total pressure is 5%. Further information on H2K can be found in [19].

During each test, the facility operating conditions like the reservoir pressure p_0 and the reservoir temperature T_0 were measured in H2K's settling chamber with a sampling rate of 50 Hz. For the measurement of reservoir pressure, the absolute pressure transducer of the UNIK 5000 series GE Druck was used with an overall accuracy of ±2.8 kPa in the measurement range between 250 kPa and 5500 kPa. For the measurement of reservoir temperature, a thermocouple type K class 1 from MTB Sensor-Technik was used that has an overall accuracy of ±1.5 K.

For the present study, the same nominal flow conditions are employed as in an earlier work with single cylindrical bodies [17]. Nominal conditions of the current tests were p_0 = 520 kPa and T_0 = 600 K at a free-stream Mach number Ma_∞ of 7.0 resulting in a unit free-stream Reynolds number of 2.0×10^6/m. Typical conditions of the experiments were a free-stream density of ρ_∞ = 0.00728 kg/m^3, a free-stream velocity of v_∞ = 1046 m/s and a free-stream dynamic pressure of q_∞ = 3981 Pa.

2.2. Model setup

Spheres, spherical caps, boxes, plates, cylinders, cones, L-shape and U-shape bodies were used as test objects with different aspect ratios. These objects were selected, as the simple bodies are used as typical primitives in common re-entry analysis tools such as ESA's DRAMA [20]. All test objects were crafted from stainless steel. The masses of the objects were measured with a precision scale, and the moments of inertia were computed based on the actual masses and dimensions. Table 1 shows the model properties' actual values for width w (or diameter for bodies with circular cross-section), height h, length l, mass m, transverse inertia I_{yy} and the standardized material number.

A reference frame is defined to determine the aerodynamic coefficients, e.g. for the lift force C_L, drag force C_D and pitching moment C_M. The origin of its right-handed global coordinate system (GCS) is spatially fixed in the centre of nozzle's exit plane. It has the positive x-axis pointing downstream, the y-axis in the transverse direction and the positive z-axis pointing vertically up. A body-fixed local coordinate system (LCS) is defined in the centre of gravity (CoG) of the free-flight object. An object is orientated in the zero flight attitude in such a way that the normal vector of its base surface is reversed to the global x-axis and its length, width and height are the corresponding dimensions to the Cartesian coordinates x, y, z, respectively. In the present experimental setup, the motions of the test objects are expected to arise in an xz-plane, so that the subsequent motion analysis is treated as 3DoF and the pitch angle ϑ is the influence factor of interest in this study. Its positive direction of rotation is clockwise when viewed along the y-axis.

2.3. Free-flight technique

A free-flight technique that allows an entirely free movement of the model in flow was applied for the present tests. This technique has already been used successfully in several studies with single or multiple blunt bodies as in [12, 17, 10, 18].

Table 1. Actual model properties

Geometry	Model	w [mm]	h [mm]	l [mm]	m [g]	I_{yy} [10^{-4} $kg\,m^2$]	Material number
Sphere	S50	50.04			501.07	1.2547	1.4125
Spherical cap	H50	50.10		25.19	249.76	0.4065	1.4112
Box	B50	50.20	50.19	50.20	962.31	4.0410	1.4112
Box	B51	50.18	50.18	100.18	1922.41	20.1117	1.4112
Box	B52	50.19	50.17	200.14	3839.96	136.2324	1.4112
Plate	P25	50.17	25.16	100.15	959.07	8.5222	1.4112
Plate	P12	50.17	12.72	100.23	480.92	4.0910	1.4112
Cylinder	C50	50.15		50.15	750.58	2.7529	1.4112
Cylinder	C52	50.14		200.18	3004.37	105.0467	1.4112
Cone	K50	49.90		50.18	254.23	0.4872	1.4112
Cone	K51	49.93		100.10	511.67	2.4946	1.4112
Cone	K52	50.00		200.10	1026.72	17.2274	1.4112
L-shape	L50	50.18	50.20	50.17	420.06	1.7799	1.4112
U-shape	U50	50.20	50.20	50.21	601.16	3.0832	1.4112

An illustration of the experimental setup in the H2K's test section using the free-flight technique is provided in Figure 1, where the initial orientations of a plate, an L-shape body and a U-shape body on the model dropping system are shown in the upper right corner, for example. In the beginning, the measurement chamber is in vacuum condition and the test object is held by an electromagnet located at the ceiling of the chamber. To enable a precise alignment and angle adjustment of the model, a fixed mounting support is employed together with an adjustable angle mounting plate to cover a large variety of initial pitch angles ϑ_0. When the free jet is stable, the model is released from the holder and falls in vacuum. When passing the top shear layer, the increasing total pressure causes a rotation of the body. Subsequently, the effective test time of about 0.1 s begins as soon as the model is completely within the homogeneous core flow and ends as soon as it reaches the edge of the core flow. At the end, the model crosses the lower part of the shear layer before it is caught at the bottom of the test section. For the present experimental setup, two or three model releases per run of the wind tunnel were realized, which benefit a reduction of operation costs and time. A time delay was satisfied between the drops in order to ensure a steady state of the free jet for each free flight.

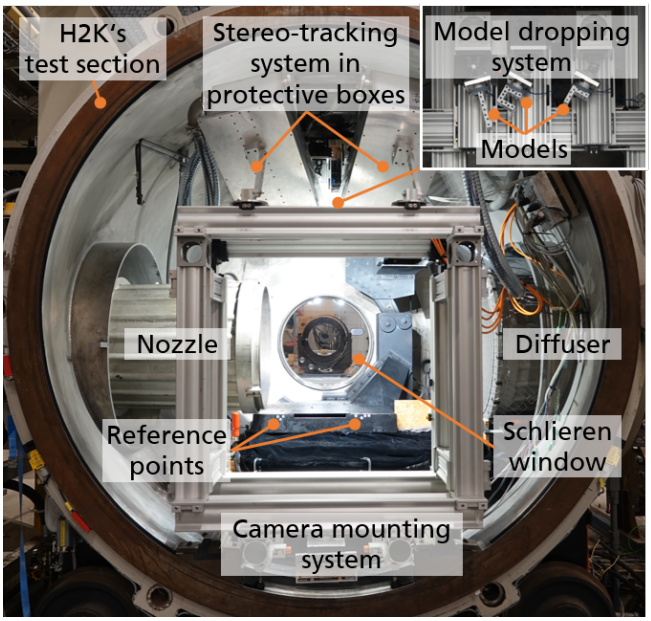

Fig. 1. Experimental setup in H2K's test section

2.4. Instrumentation

To characterise the flow field around the test objects, high-speed schlieren videography was used with a single-path Z-type setup as in [21]. This setup was equipped with a 1000 W xenon arc lamp as a light source and a Photron FASTCAM APX-RS model 250K high-speed camera for image recording. The camera was set to a frame rate of 3 kHz at full 1024 × 1024 pixels resolution and an exposure time of 2 µs.

To reconstruct the three-dimensional flight trajectory and attitude of the free-flying objects, a high-speed stereo-tracking system based on the detection of marker points was applied with two synchronously recording cameras in stereoscopic arrangement. Both cameras were the Photron FASTCAM SA-X2 model 1080K. The cameras were set to the full 1024 × 1024 pixels resolution at a frame rate of 12 kHz. Each camera was outfitted with a 24-mm-focal-length lens ensuring the observation of a measurement volume of 600 × 640 × 640 mm. To ensure sufficient illumination, each camera was equipped with four 86 W plus four 38 W high-power LEDs on a capacitive cooling ring mounted concentrically on the optical window of the protective box.

2.5. Data processing

For determining the position and orientation of a test object in 3D space, the recorded sequence of synchronous image pairs from the stereo-tracking cameras was processed using the commercial stereo-tracking software ARAMIS Professional 2017, which uses digital image correlation (DIC) based on a random arrangement of marker points. ARAMIS is applied to determine the three positions in streamwise (x), spanwise (y) and vertical (z) direction as well as the roll (φ), pitch (ϑ) and yaw (ψ) angles of the model in relation to the GCS. With the present setup, a calibration deviation of less than 1 µm is achieved. The true accuracies of the stereo-tracking system including the influence of the flow and a detailed description of the data processing can be found in [18].

The resulting time-resolved motion data are employed to determine the translational and angular velocities and accelerations by filtering and differentiating. Discrete differentiations are performed using central finite difference quotient. A conventional Savitzky-Golay filter with a linear polynomial and a window length of 201 data points was used to smooth the data before each differentiation and the determination of the aerodynamic coefficients.

The force and moment coefficients are calculated with the expressions from [18], whereby the reference area S_{ref} is defined as the projected area of the respective geometry at a zero flight attitude. For the reference length l_{ref}, the width of the model is applied as given in Table 1. To determine the lift coefficient, the vertical force component is separated from gravity.

An uncertainty analysis was carried out for the measurement data by estimating the uncertainties of the measurement chain and their influence on the motion derivatives and aerodynamic coefficients. For this purpose, Monte Carlo simulations were performed with 4000 samples using the data processing procedure described above and the total uncertainties of the relevant quantities such as Ma_∞, p_0, κ, m, I_{yy}, S_{ref}, l_{ref}, x, z and ϑ.

To determine a complete aerodynamic database for all pitch angles, a non-linear regression analysis is performed for the present experimental data by means of trigonometric functions to estimate relations between aerodynamic coefficients and the independent variables pitch angle ϑ and aspect ratio λ. The experimental data of several tests are fitted by a method of successive approximation to determine the function parameters. In doing so, the method of least absolute residuals is used, as this is less sensitive to the presence of outliers than the more commonly used method of least squares regression.

3. EXPERIMENTAL RESULTS

In the following, the experimental results of the cylinders with aspect ratios of $\lambda = \{4, 2, 1\}$ and different initial pitch angles are presented, whereby the measurement data for the cylinder with an aspect ratio of 2 originate from a previous work [17]. Furthermore, the mathematical functions from the regression analysis are shown below.

3.1. Flow topology

Figure 2 illustrates a representative schlieren image sequence of a free-flying elongated cylinder that has an aspect ratio of 4 with an initial pitch angle of 105°, whereby the duration between the first and last image is 1/30 s. The characteristically detached bow shock for flow topologies of blunt bodies in the supersonic flow regime can be seen here, while low-density-gradient flow features such as the wake region and compression waves are not visible due to the low sensitivity of the Z-type schlieren system. It is also apparent from the schlieren images that the cylinder undergoes a counter-clockwise pitch rotation induced by the shear layer of the free jet, as described in previous studies such as [17]. In this test case, the body edge protrudes more and more into the flow during free flight, which is why the the shock stand-off distance decreases and the shock curvature in the vicinity of the edge increases. As a result, the flow topology depends strongly on the flight attitude of the body.

3.2. Model motion

The measurement data show that the out-of-plane motions of the present tests are substantially smaller than the corresponding in-plane motions and are therefore neglected in the following analysis. Figure 3 depicts the flight trajectories of all tests with the elongated cylinder in the xz-plane with respect to the centre of the nozzle exit, whereby the flow regions of the free jet from experimental flow characterisations are also shown as grey contour layers. Two release devices are used for this free-flight tests, whereby the initial positions were varied slightly. At first glance, the streamwise displacement is very different between the various configurations, which is due to different residence time in the jet core and motion behaviour of the models. This observation can be explained by the change in the frontal wetted area and the aerodynamic coefficients, which depend on the pitch angle as shown in previous studies [17, 18]. In doing so, this figure indicates that the greater the aspect ratio of the body, the greater the influence of the the pitch angle on the aerodynamic loads. This is consistent with the earlier findings of [22].

3.3. Aerodynamic forces & moments

As a result of the data processing described in Section 2.5, the aerodynamic coefficients are determined based on the motion data. Drag force, lift force and pitching moment coefficients of the elongated cylinder C52 with an initial pitch angle of 105° are plotted against the time in Figure 4 for a representative configuration, whereby the time frame has its origin at the moment when the test article is completely within the core

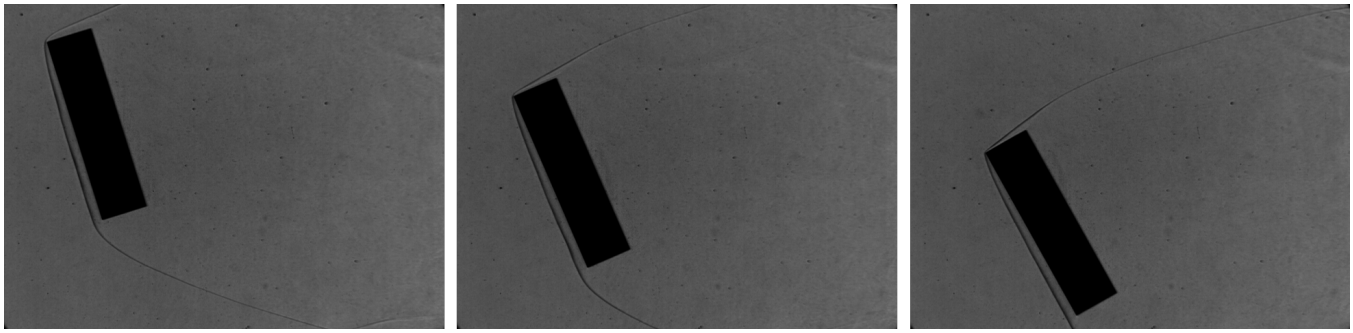

Fig. 2. Example of schlieren image sequence showing the motion behaviour in free flight for a cylinder with $\lambda = 4$ and $\vartheta_0 = 105°$

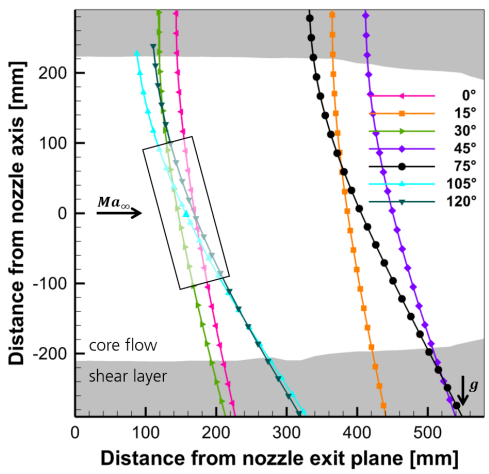

Fig. 3. Several flight trajectories of cylinder with an aspect ratio of 4 and different initial pitch angle relating to the flow regions of H2K's Mach-7 nozzle; cyan triangle indicates position of the cylinder at a specific moment

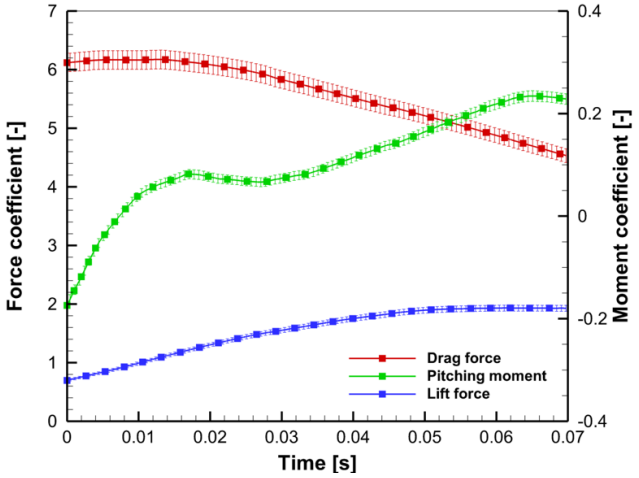

Fig. 4. Representative evolution of aerodynamic coefficients of a cylinder with $\lambda = 4$ and $\vartheta_0 = 105°$ in core flow including total measurement uncertainties

flow for the first time. In addition, error bars representing estimated total uncertainties are provided in Figure 4, whereby the relative average uncertainties are 2% for C_D, 2% for C_L and 4% for C_M based on their peak values. Significant deviations for the pitching moment coefficients can be seen at the beginning of the graph in the Figure 4, which are not an effect of the aerodynamic behaviour. These deviations can be explained by the fact that the first and also the last values are influenced by measurement points captured within the jet shear layer during the data processing. As expected, the aerodynamic coefficients of the in-plane motion shown in the line chart change considerably over time.

In Figure 5, the drag and lift coefficient of all tests performed with cylinders of different aspect ratios are depicted as a function of the pitch angle, whereby differently coloured lines with symbols correspond to the measurement data of various free-flight tests. From these graphs it can be see that both force coefficients are dependent on the pitch angle and that this effect increases with higher aspect ratios. In contrast, the drag coefficient of the cylinder in axial flow ($\vartheta = 0°$) related to the base area is almost the same for all aspect ratios. In the case of cylinders in cross flow ($\vartheta = 90°$), their drag coefficient multiplies to the same extent as their aspect ratio, which is why the the drag coefficient related to the projected lateral surface area is the same. Hence, the aspect ratio of cylinders in axial and cross flow has no significant effect on the force coefficients based on the actual frontal wetted area.

Additionally, the fitted trigonometric series from the regression analysis are presented in Figure 5, while Equations 1 and 2 provide their mathematical expressions for the drag and lift coefficients as functions of the pitch angle and aspect ratio. The symmetry of the cylinders is also taken into account when selecting the angular frequency of the sine and cosine terms. As a result of the fitting, the mean absolute residuals are just acceptable at 0.035 for C_D and 0.036 for C_L. However, these fits have some deviations beyond the total uncertainty of the experimental data, whereby the fits of

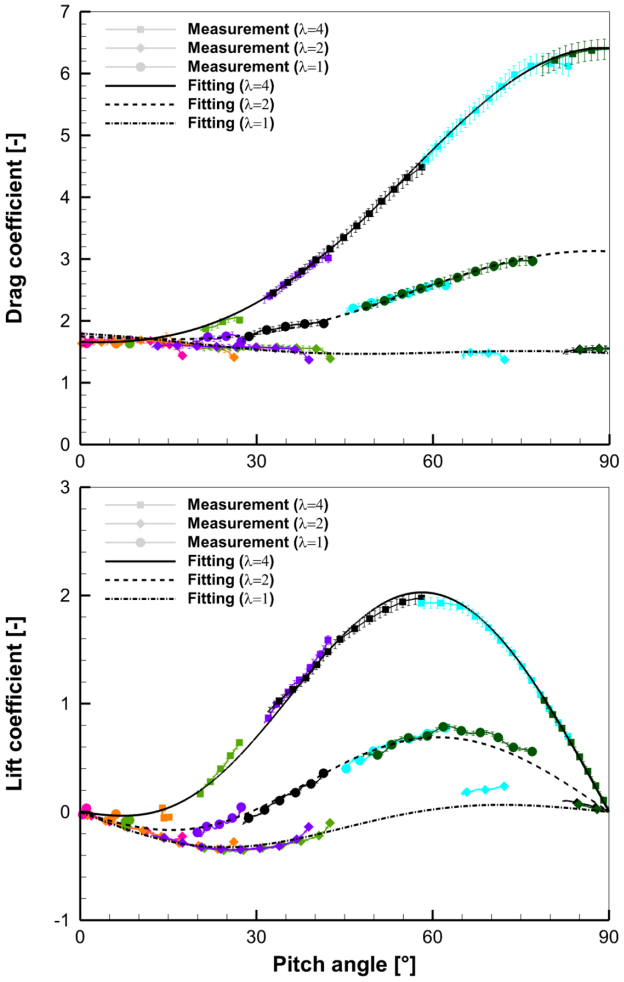

Fig. 5. Aerodynamic force coefficients of cylinders as a function of pitch angle based on experimental data as well as curve fitting for different orientations and aspect ratios

the drag coefficients for different aspect ratios close to a zero pitch angle and the lift coefficients for $\lambda = 1$ in the pitch angle range from 65° to 75° show clear discrepancies. To improve the fitting results, the number of function parameters and terms can be increased or more appropriate function types can be selected for regression analysis based on the given experimental data. This is planned for the further analysis. In order to develop better mathematical expressions for the aerodynamic coefficients, a suitable approach would be the use of spherical harmonics as in [23] or sparse identification of nonlinear dynamics (SINDy) as in [24].

$$C_D(\vartheta,\lambda) = (0.716\lambda + 0.836) - 0.061 \cdot \sin(4\vartheta) \\ -(0.844\lambda - 1) \cdot \cos(2\vartheta) + 0.084\lambda \cdot \cos(4\vartheta) \quad (1)$$

$$C_L(\vartheta,\lambda) = (0.577\lambda - 0.743) \cdot \sin(2\vartheta) \\ -0.192\lambda \cdot \sin(4\vartheta) - 0.020\lambda \cdot \sin(6\vartheta) \quad (2)$$

4. AERODYNAMIC MODEL

The fragmentation of space debris entering the atmosphere produces several fragments of different shapes, sizes and relative positions to each other. These fragments follow individual trajectories, which are influenced not only by their inherent aerodynamic behaviour but also by aerodynamic interaction with other fragments. For this purpose, an empirical fragment-flow interaction model is developed in the present work, which considers the aerodynamics with a focus on the supersonic/hypersonic flow regime and thus the motion behaviour of individual fragments on a physical basis in contrast to common debris cloud models. This empirical aerodynamic model treats the aerodynamic interactions as multiple separate two-body problems according to [10] to cover a complete consideration of fragment interactions. Thereby, the largest object after fragmentation is the parent body and the others are the child bodies. The interactions between the child fragments are neglected as they are minor compared to the influence of the largest object. Moreover, it is assumed that this is a restricted two-body problem in which the impact of the parent fragment on the child ones is considered, but not vice versa. This assumption can be explained by the finding from an earlier study with multi-body arrangements, where the aerodynamic loads of the trailing bodies vary significantly with their relative streamwise and lateral distance to the leading ones, while the impact on the leading body is negligible [12]. This is not surprising since the flow conditions are supersonic. Unlike the fragment-flow interaction model of [10], the shape and orientation of the fragments should be take into account. A solid rationale for this assumption comes from [22, 17, 18], since wind tunnel experiments with single bodies have shown that the drag force, lift force and pitching moment coefficients are significantly dependent on their geometry and attitude. In addition, experiments conducted with multiple bodies have revealed that the shape and orientation of the trailing objects strongly influence their flight trajectories and that the strong lateral separation of the trailing objects is due to the two effects of the shock-shock interaction and the inclination-induced lift force [12, 8].

Experimental data provide the foundation of this novel database-based aerodynamic model, for which the aerodynamic coefficients should be expressed as mathematical functions from the regression analysis (see e.g. Equations 1 and 2). The database consists of two parts with single-body and multi-body datasets of the various geometries as given in Table 1. For the modelling of re-entry events, the single-body data applies to parent fragments, independent child fragments and the intact object of space debris before

the first breakup, while the multi-body data is used for dependent child fragments. To determine the aerodynamic loads of the dependent child fragments, the aerodynamic interaction of two objects is treated as configuration of a leading sphere and the respective child object as trailing body. It can be argued that this assumption is plausible because the bow shock shape, in particular its shock radius and angle, of the leading parent fragment downstream increasingly approximates that of a sphere with the same projected radius as the actual fragment. The projected radius is the maximum dimension of the respective body relative to its centre of gravity in the plane under consideration. Furthermore, the findings of a previous investigation supports this assumption, as it demonstrates that the geometry of the neighbouring body has no significant effect on the lateral motion of the influenced body for side-by-side configurations of differently shaped objects [25]. The multi-body data ensure a variation of the orientation angles, the size ratio and the position of the child fragment relative to the parent one, while the single-body data cover a variation of the orientation angles of the child fragment. However, the current version of the aerodynamic database is accomplished for 3DoF motion analysis, whereby the approach can also be extended with further data, e.g. for 6DoF motion.

Since the geometry of the space debris object is modelled as a combination of different primitives in common object-oriented re-entry analysis tools, the superposition of aerodynamic coefficients for complex geometries (using L-shape and U-shape bodies) will be investigated based on the coefficients of primitives and considered for this aerodynamic model. In addition, rarefaction effects on the aerodynamic coefficients will be taken into account by a Knudsen number correction based on data from literature such as [26] for the aerodynamics of the space debris object for high altitudes before the first atmospheric breakup. Finally, this empirical fragment-flow interaction model will be used for the aerodynamic modelling in flight dynamic simulations of a satellite reference configuration considering fragmentation and individual trajectories of several objects. This is part of a further work package of the TEMIS-DEBRIS project.

5. CONCLUSION

In this study, an aerodynamic model for the atmospheric entry of space debris is developed based on aerodynamic databases, which considers both the influence of the unsteady flight attitude and the aerodynamic interactions between multiple bodies on the motion of the debris fragments. To this end, a series of free-flight tests at Mach 7 were carried out at DLR's H2K in Cologne with various common geometries for debris fragments such as spheres, spherical caps, boxes, plates, cylinders, cones and more complex bodies. A stereo-tracking system was used to measure high-speed 6DoF motion data consisting of time-resolved positions and orientation angles of the test objects. Comprehensive data processing was used to determine the motion derivatives including the aerodynamic coefficients, which were subsequently used in a regression analysis to determine their trigonometric functions with respect to the pitch angle and aspect ratio. The results of cylinders with different aspect ratios are shown in the present paper.

In addition, multi-body experiments with different geometries in a wide range of relative distances and orientations are planned to expand the database in order to cover the interaction of multiple fragments after atmospheric breakups. For this purpose, the trailing objects will be instrumented with a force moment-type balance to measure the aerodynamic loads.

6. REFERENCES

[1] ESA Space Debris Office, "ESA's annual space environment report," Tech. Rep. GEN-DB-LOG-00288-OPS-SD, European Space Agency, Darmstadt, Sept. 2023.

[2] ESA Space Mitigation Working Group, "ESA space debris mitigation requirements," Tech. Rep. ESSB-ST-U-007, European Space Agency, Darmstadt, Oct. 2023.

[3] Quinn R. Passey and H. J. Melosh, "Effects of atmospheric breakup on crater field formation," *Icarus*, vol. 42, no. 2, pp. 211–233, May 1980.

[4] Monal Patel and Salvador Navarro-Martinez, "Heat transfer to proximal cylinders in hypersonic flow," *Physics of Fluids*, vol. 35, no. 036125, Mar. 2023.

[5] Dániel G. Kovács, Guillaume Grossir, Grigorios Dimitriadis, and Olivier Chazot, "Space debris interaction across a two-dimensional oblique shock wave," *Experiments in Fluids*, vol. 64, no. 8, Aug. 2023.

[6] David Leiser, Stefan Löhle, Fabian Zander, David R. Buttsworth, Rishabh Choudhury, and Stefanos Fasoulas, "Analysis of reentry and break-up forces from impulse facility experiments and numerical rebuilding," *Journal of Spacecraft and Rockets*, vol. 59, no. 4, pp. 1276–1288, July 2022.

[7] Vincente Cardona and Viviana Lago, "Aerodynamic forces of interacting spheres representative of space debris re-entry: Experiments in a supersonic rarefied wind-tunnel," *Acta Astronautica*, vol. 191, pp. 148–159, Feb. 2022.

[8] Seong-Hyeon Park, Junemo Kim, Ilsung Choi, and Gisu Park, "Experimental study of separation behavior of two bodies in hypersonic flow," *Acta Astronautica*, vol. 181, pp. 414–426, Apr. 2021.

[9] Thomas J. Whalen and Stuart J. Laurence, "Experiments on the separation of sphere clusters in hypersonic flow," *Experiments in Fluids*, vol. 62, no. 4, Mar. 2021.

[10] Paul J. Register, Michael J. Aftosmis, Eric C. Stern, Joseph M. Brock, Patrick M. Seltner, Sebastian Willems, Ali Gülhan, and Donovan L. Mathias, "Interactions between asteroid fragments during atmospheric entry," *Icarus*, vol. 337, no. 113468, Feb. 2020.

[11] Tao Li, JingXia Sui, Sheng Gong, and ChuiJie Wu, "Dynamical separation of rigid bodies in supersonic flow," *Science China Technological Sciences*, vol. 58, no. 12, pp. 2110–2121, Dec. 2015.

[12] Patrick M. Seltner, Sebastian Willems, and Ali Gülhan, "Aerodynamic interactions of blunt bodies free-flying in hypersonic flow," *Experiments in Fluids*, vol. 65, no. 80, May 2024.

[13] Stuart J. Laurence and R. Deiterding, "Shock-wave surfing," *Journal of Fluid Mechanics*, vol. 676, pp. 396–431, Apr. 2011.

[14] Hilding Elmqvist, Martin Otter, Andrea Neumayr, and Gerhard Hippmann, "Modia - Equation based modeling and domain specific algorithms," in *14th Modelica Conference*, Linköping, Sweden, Sept. 2021, vol. 181, pp. 73–86, Linköping University Electronic Press.

[15] Andrea Neumayr and Martin Otter, "Modelling and simulation of physical systems with dynamically changing degrees of freedom," *Electronics*, vol. 12, no. 3, pp. 500, Jan. 2023.

[16] Lâle Evrim Briese, Andreas Klöckner, and Matthias Reiner, "The DLR Environment Library for multidisciplinary aerospace applications," in *12th International Modelica Conference*, Prague, Czech Republic, May 2017, vol. 132, pp. 929–938, Linköping University Electronic Press.

[17] Patrick M. Seltner, Sebastian Willems, Ali Gülhan, Eric C. Stern, Joseph M. Brock, and Michael J. Aftosmis, "Aerodynamics of inclined cylindrical bodies free-flying in a hypersonic flowfield," *Experiments in Fluids*, vol. 62, no. 9, Aug. 2021.

[18] Patrick M. Seltner, Sebastian Willems, and Ali Gülhan, "Aerodynamic coefficients of free-flying cubes in hypersonic flowfield," *Journal of Spacecraft and Rockets*, vol. 56, no. 6, pp. 1725–1734, Nov. 2019.

[19] F.-J. Niezgodka, "Der Hyperschallwindkanal H2K des DLR in Köln-Porz (Stand 2000)," Tech. Rep., DLR, Köln, Jan. 2001.

[20] HTG, "Final report: Upgrade of DRAMA's Spacecraft Entry Survival Analysis codes," techreport 4000115057/15/D/SR, Hyperschall Technologie Göttingen, Bovenden, Dec. 2019.

[21] Dennis Daub, *Experimental investigation of supersonic fluid-structure interaction for future space transportation systems*, phdthesis, DLR/RWTH Aachen University, Cologne/Aachen, Sept. 2023, DLR-FB 2023-09.

[22] Travis A. Duchene and Stuart J. Laurence, "The aerodynamics of sharp- and filet-edged cylinders in high supersonic flow," *Experiments in Fluids*, vol. 66, no. 2, Jan. 2025.

[23] Flynn Hack, Andrew Lock, Gerard Armstrong, Ingo Jahn, David Buttsworth, and Fabian Zander, "Aerodynamic coefficients of a cube in hypersonic flow for all attitudes," *Journal of Spacecraft and Rockets*, pp. 1–12, Feb. 2025.

[24] Jean-Christophe Loiseau, Bernd R. Noack, and Steven L. Brunton, "Sparse reduced-order modelling: Sensor-based dynamics to full-state estimation," *Journal of Fluid Mechanics*, vol. 844, pp. 459–490, Apr. 2018.

[25] V. T. Lukashenko and F. A. Maksimov, "On the separation of two meteoroid fragments of different shapes," *Journal of Physics: Conference Series*, vol. 1479, Mar. 2020.

[26] Sighard F. Hoerner, *Fluid-dynamic drag: Practical information on aerodynamic drag and hydrodynamic resistance*, Hoerner Fluid Dynamics, Bakersfield, 2. ed. edition, 1965.